

## COMPOSITIONALLY-DRIVEN CONVECTION IN THE OCEANS OF ACCRETING NEUTRON STARS

ZACH MEDIN AND ANDREW CUMMING

Department of Physics, McGill University, 3600 rue University, Montreal, QC H3A 2T8, Canada; zmedin@physics.mcgill.ca,  
cumming@physics.mcgill.ca  
*Draft version June 16, 2022*

### ABSTRACT

We discuss the effect of chemical separation as matter freezes at the base of the ocean of an accreting neutron star, and argue that the retention of light elements in the liquid acts as a source of buoyancy that drives a slow but continual mixing of the ocean, enriching it substantially in light elements, and leading to a relatively uniform composition with depth. We first consider the timescales associated with different processes that can redistribute elements in the ocean, including convection, sedimentation, crystallization, and diffusion. We then calculate the steady state structure of the ocean of a neutron star for an illustrative model in which the accreted hydrogen and helium burns to produce a mixture of O and Se. Even though the H/He burning produces only 2% oxygen by mass, the steady state ocean has an oxygen abundance more than ten times larger, almost 40% by mass. Furthermore, we show that the convective motions transport heat inwards, with a flux of  $\approx 0.2$  MeV per nucleon for an O-Se ocean, heating the ocean and steepening the outwards temperature gradient. The enrichment of light elements and heating of the ocean due to compositionally-driven convection likely have important implications for carbon ignition models of superbursts.

*Subject headings:* dense matter — stars: neutron — X-rays: binaries — X-rays: individual

### 1. INTRODUCTION

The ocean of an accreting neutron star is composed of a variety of elements with atomic number  $Z = 6$  and larger, formed by nuclear burning of the accreted hydrogen and helium at low densities. The term ocean refers to the fact that the Coulomb interaction energy between ions is greater than the thermal energy, such that the ions behave like a liquid. The ocean is of interest as the site of long duration thermonuclear flashes such as superbursts (Cumming & Bildsten 2001; Strohmayer & Brown 2002; Kuulkers 2004) and intermediate duration bursts (in 't Zand et al. 2005; Cumming et al. 2006), non-radial oscillations (Bildsten & Cutler 1995; Piro & Bildsten 2005), and because the matter in the ocean eventually solidifies as it is compressed to higher densities by ongoing accretion, and so determines the thermal, mechanical and compositional properties of the neutron star crust (Haensel & Zdunik 1990; Brown & Bildsten 1998; Schatz et al. 1999).

At the base of the ocean, matter freezes as it is compressed by continuing accretion, becoming part of the solid crust. Horowitz et al. (2007) carried out molecular dynamics simulations of the freezing of a mixture of 17 species taken from a calculation of rp-process hydrogen and helium burning and hence representative of the kind of mixture expected to make up the ocean of an accreting neutron star (Schatz et al. 2001; Gupta et al. 2007). They found that this mixture underwent chemical separation during crystallization, such that light elements (charge number  $Z \lesssim 20$ ) were preferentially left behind in the liquid, whereas heavier elements were preferentially incorporated into the solid. In a previous paper (Medin & Cumming 2010, hereafter Paper I) we showed that this result can be understood by generalizing previous work using fits to the free energies of the liquid and solid states of binary and tertiary plasmas.

In this paper, we address the implications of chemi-

cal separation for the structure and composition of the ocean. Horowitz et al. (2007) raised the question of what the steady-state ocean would look like, since the matter entering the crust is enriched in certain elements compared to others, and therefore different from the mean ocean composition. We investigate this question here, and argue that the retention of light elements in the liquid acts as a source of buoyancy that drives a slow but continual mixing of the ocean, enriching it substantially in light elements and leading to a relatively uniform composition with depth. The steady state arises as the ocean enriches in light elements to the point where the composition of the solid that forms upon freezing matches the composition of matter entering the top of the ocean.

One motivation for studying this problem comes from models for superbursts which involve thermally-unstable carbon burning in the deep ocean of the neutron star (Cumming & Bildsten 2001; Strohmayer & Brown 2002). The energy release in these very long duration thermonuclear flashes, inferred from fitting their lightcurves (Cumming et al. 2006), corresponds to carbon fractions of  $\approx 20\%$ . This has been challenging to produce in models of the nuclear burning of the accreted hydrogen and helium. If the hydrogen and helium burn unstably, the amount of carbon produced is  $\lesssim 1\%$  (Woosley et al. 2004), and whereas stable burning can produce large carbon fractions (Schatz et al. 2003), time-dependent models do not show stable burning at the  $\approx 10\%$  Eddington accretion rates of superburst sources (although observationally, superburst sources show evidence that much of the accreted material may not burn in Type I bursts; in 't Zand et al. 2003).

Perhaps even more problematic than making enough carbon is that carbon ignition models for superbursts require large ocean temperatures  $\approx 6 \times 10^8$  K at the ignition depth, which are difficult to achieve in standard models of crust heating (e.g., Cumming et al. 2006; Keek

et al. 2008). Similarly, Brown & Cumming (2009) inferred a large inwards heat flux in the outer crust of the transiently-accreting neutron stars MXB 1659-29 and KS 1731-260 by fitting their cooling curves in quiescence. Both of these observations imply an additional heating source in the outer crust or ocean is needed. In this paper, we begin to address the question of to what extent chemical separation could enrich the ocean in carbon and other light elements, or provide a heat source that could alleviate some of the difficulty of matching the observations of superbursts and transient cooling.

We begin in §2 by reviewing the physics of chemical separation, and discussing the timescales on which accretion, crystallization, diffusion, sedimentation, and convection occur, leading us to a picture of compositionally-driven convection. In §3 we calculate the structure of the steady-state ocean for two simplified models: first, accretion of a two-component mixture composed of Se and either O or Fe; and second, accretion of a mixture of H and He which then burns to produce these heavier-element mixtures. In §4 we consider the effect of the mixing on the thermal profile, and calculate the heating of the ocean due to the convective transport of light elements outwards. Finally, in §5 we discuss the implications of our results.

## 2. MIXING PROCESSES IN THE OCEAN

### 2.1. Phase diagrams and chemical separation

The degree of chemical separation on freezing can be understood from the phase diagram for the mixture. Figure 1 shows two examples of phase diagrams, calculated as described in Paper I. The upper panel is for a mixture of  $^{56}\text{Fe}$  ( $Z = 26$ ) and  $^{79}\text{Se}$  ( $Z = 34$ ), the lower panel for a mixture of  $^{16}\text{O}$  ( $Z = 8$ ) and  $^{79}\text{Se}$  ( $Z = 34$ ). In the first case the diagram is of azeotrope type; in the second case, for which the ratio of atomic numbers  $Z$  is greater, the diagram is a more complicated eutectic type. In each case, the x-axis shows the number fraction of Se and the y-axis shows the inverse Coulomb coupling parameter for the light species (Fe or O respectively)  $\Gamma^{-1}$ . The Coulomb coupling parameter for species  $i$  is

$$\begin{aligned} \Gamma_i &= \frac{Z_i^{5/3} e^2}{k_B T} \left( \frac{4\pi\rho Y_e}{3m_p} \right)^{1/3} \\ &= 204 \rho_9^{1/3} \left( \frac{T_8}{3} \right)^{-1} \left( \frac{Z_i}{34} \right)^{5/3} \left( \frac{Y_e}{0.43} \right)^{1/3}, \end{aligned} \quad (1)$$

where  $Z_i$  is the charge of the ion,  $Y_e = \langle Z \rangle / \langle A \rangle$ ,  $\langle Z \rangle$  and  $\langle A \rangle$  are the average charge and mass per ion of the mixture,  $\rho_9 = \rho / (10^9 \text{ g/cm}^3)$  the density, and  $T_8 = T / (10^8 \text{ K})$  the temperature. For a single species of ion, solidification occurs when  $\Gamma_1 > \Gamma_m \approx 175$  (e.g., Potekhin & Chabrier 2000). Note that for a given  $\rho$  and  $T$  (or depth in the star),  $\Gamma_i$  is nearly constant with composition. As a fluid element is compressed by accretion to higher density,  $\Gamma_1$  increases, moving down in the phase diagram. The shaded regions represent unstable regions of the phase diagram. A fluid element with composition and  $\Gamma_1$  that lies inside the unstable region will undergo phase separation, separating into two phases with compositions on each side of the unstable region. In this way, chemical separation occurs. Note that the curves that

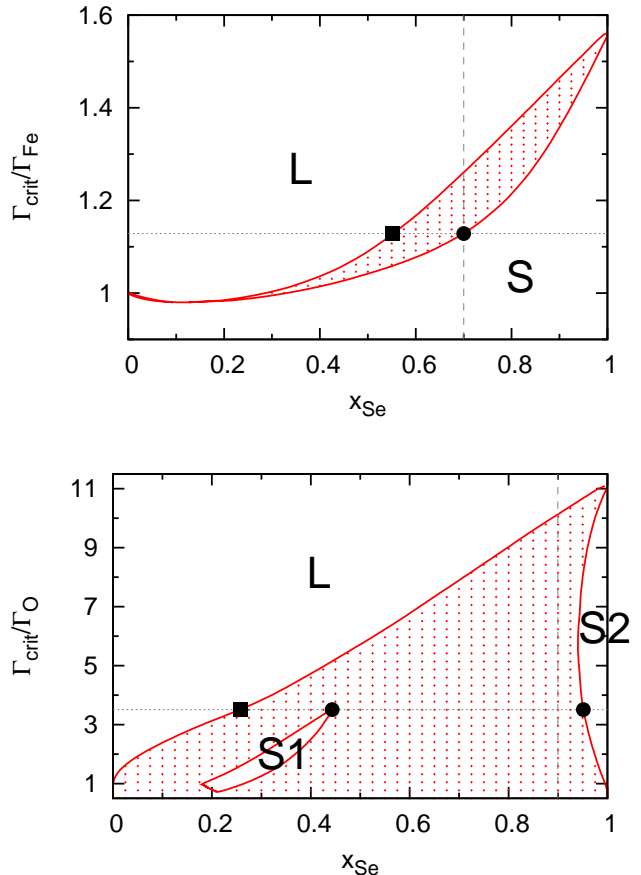


FIG. 1.— (Color online) The phase diagram for crystallization of an  $^{56}\text{Fe}$ - $^{79}\text{Se}$  mixture (top panel) and an  $^{16}\text{O}$ - $^{79}\text{Se}$  mixture (bottom panel) in a  $T = 3 \times 10^8 \text{ K}$  ocean. The Coulomb coupling constants  $\Gamma_{\text{Fe},\text{O}}$  are given in terms of  $\Gamma_{\text{crit}} \approx 175$ , the value at which a single-species plasma crystallizes. The stable liquid region of each phase diagram is labeled ‘L’, the stable solid region(s) are labeled ‘S’ or ‘S1’ and ‘S2’, and the unstable region is filled with plus symbols. Additionally, in each panel the composition at the top of the ocean is marked by a vertical dashed line, the ocean-crust boundary is marked by a horizontal dotted line, the composition of the liquid at the base of the ocean is marked by a filled square, and the composition of the solid(s) in the outer crust are marked by filled circles.

bound the unstable region are commonly referred to as the liquidus and solidus curves, respectively. A liquid with composition of the liquidus curve at a given  $\Gamma_1$  is in equilibrium with the solid which has the composition of the solidus curve at that  $\Gamma_1$ .

Now consider a particular mixture of Fe and Se entering the top of the ocean with  $x_{\text{Se}} = 0.7$  (this corresponds to 77% Se and 23% Fe by mass), indicated by the vertical dashed line in the upper panel of Fig. 1. In steady state, the solid forming at the top of the crust must have this same composition, so that the freezing point must lie at  $\Gamma_m / \Gamma_{\text{Fe}} \approx 1.1$  as marked by the filled circle in Fig. 1. The corresponding liquid composition in equilibrium with the solid at this  $\Gamma_{\text{Fe}}$  is indicated by the solid square. The phase diagram shows that the liquid at the base of the ocean must have a composition  $x_{\text{Se}} \approx 0.56$  (63% Se by mass) in order to make the solid composition demanded by steady state.

The lower panel of Fig. 1 shows a more complicated example. The vertical dotted line marks an incoming composition with  $x_{\text{Se}} = 0.9$  (corresponding to 98% Se and 2% O by mass). In this case, there is no single solid phase with this composition. Instead, at  $\Gamma_m/\Gamma_O \approx 3.5$ , a mixture of two solid phases indicated by the filled circles forms, and the liquid at the base of the ocean has  $x_{\text{Se}} \approx 0.25$  (63% Se by mass). Again, in order to reach steady state, the base of the ocean must adjust its composition until it is significantly enriched in light elements compared to the composition at the top of the ocean.

## 2.2. Crystallization of solid particles

To see how the ocean is able to adjust its composition profile to achieve steady state, we first note that solid particles crystallize and sediment out rapidly compared to the accretion timescale on which matter is compressed. The accretion time is  $t_{\text{accr}} = H_P/v_{\text{accr}} = y/\dot{m}$  or

$$t_{\text{accr}} = 3.2 \frac{y_{12}}{\dot{m}_4} \text{ yrs} = 7.2 \frac{\rho_9^{4/3}}{\dot{m}_4} \left( \frac{Y_e}{0.43} \right)^{4/3} \left( \frac{g_{14}}{2.45} \right)^{-1} \text{ yrs}, \quad (2)$$

where  $H_P = P/\rho g = y/\rho$  is the pressure scale height,  $y$  is the column depth,  $\dot{m}$  is the local accretion rate per unit area and in the last step we use the fact that the pressure in the ocean is dominated by relativistic degenerate electrons. We scale to a typical rate  $\dot{m}_4 = \dot{m}/(10^4 \text{ g cm}^{-2} \text{ s}^{-1})$  (to set the scale note that the Eddington rate is  $\dot{m}_{\text{Edd}} \approx 10^5 \text{ g cm}^{-2} \text{ s}^{-1}$ ). We choose the gravity  $g_{14} = g/(10^{14} \text{ cm/s}^2) = 2.45$  corresponding to a  $1.4 M_\odot$ ,  $R = 10 \text{ km}$  neutron star.

First, consider crystallization. The nucleation rate, the rate at which solid clusters of a size large enough to be stable are formed, is not currently well understood. Theory typically predicts nucleation rates orders of magnitude smaller than experiment or simulations indicate (see Vehkamäki 2006). For an OCP for example, the nucleation rate at  $\Gamma_1 = 300$  from the theoretical model of Ichimaru et al. (1983) is  $\sim 10^{-6}$  of its value from the simulation of Daligault (2006b). Cooper & Bildsten (2008) recently derived a value within a factor of 10 of the simulations, but their formulation predicts the formation of stable solid clusters even at  $\Gamma_1 < 175$  when the liquid phase should be absolutely stable with respect to the solid. Taking the Ichimaru et al. (1983) results, we find that the amount of undercooling necessary for the nucleation rate to become comparable to the accretion rate is  $\Gamma_1 - \Gamma_m \sim 0.1\Gamma_m$ , but given that the theory underpredicts the simulation results, the amount of undercooling required is probably much less than this. Additionally, at the base of the ocean solid clusters do not need to wait for nucleation sites to form but can crystallize on the existing crust.

Once a cluster forms it increases in size at the crystallization velocity which is of order  $v_{\text{crys}} \sim \omega_p a$  (e.g., Kelton, Greer, & Thompson 1983), where  $a$  is the mean ion spacing and  $\omega_p$  is the ion plasma frequency given by  $\omega_p = \sqrt{4\pi\rho}(Y_e e/m_p) = 1.4 \times 10^{19} \rho_9^{1/2} (Y_e/0.43) \text{ rad/s}$ . In a multicomponent plasma crystal growth is slower, since as a solid cluster grows chemical separation means that the liquid surrounding the cluster is depleted more and more of the particles necessary to form the solid.

The crystallization rate therefore depends on the rate at which diffusion can replenish the depleted particles. In a liquid with  $100 < \Gamma < 300$ , where  $\Gamma = \langle Z^{5/3} \rangle \Gamma_i / Z_i^{5/3}$  is the *average* Coulomb coupling constant, the diffusion coefficient for species  $i$  is

$$D \approx 8 \left( \frac{\langle Z \rangle}{Z_i} \right)^{2/3} \omega_p a^2 \Gamma^{-2.5} \text{ cm}^2/\text{s} \quad (3)$$

(Horowitz et al. 2010; see also Daligault & Murillo 2005). We assume that to bind to a cluster, new material must travel a distance  $l$  equal to the current size of the cluster; in this case, the cluster growth time is  $l^2/D \approx 10^{-4} \omega_p^{-1} (l/a)^2 (\Gamma/100)^{2.5}$ . For a solid cluster of  $N_s$  particles,  $(l/a)^2 \approx N_s^{2/3}$ .

Therefore as soon as the mixture encounters the liquidus line in the phase diagram, we expect solid particles to rapidly form and grow. Once formed, the solid particles will quickly sediment out. We estimate the sedimentation velocity for solid clusters following Bildsten & Hall (2001) and Brown et al. (2002). The sedimentation velocity is given by the Einstein relation

$$v_{\text{sed}} \simeq \frac{D}{k_B T} A_s N_s m_p g \frac{\Delta Y_e}{Y_e}, \quad (4)$$

where  $\Delta Y_e/Y_e = 1 - Y_{e,s}/Y_{e,l}$  is the contrast between  $Y_e$  for the solid particles and the background fluid. Note that in Eq. (4) we have neglected the contribution of the ions to the buoyancy force. Usually this amounts to a  $\sim 10\%$  correction; but when  $\Delta Y_e = 0$  this is the dominant term (Mochkovitch 1983). We use the Stokes-Einstein relation to estimate the mobility  $D/(k_B T) = (4\pi\eta a N_s^{1/3})^{-1}$ , where the OCP shear viscosity is  $\eta \approx 0.2\rho\omega_p a^2 (\Gamma/100)^{1.5} \text{ g cm}^{-1} \text{ s}^{-1}$  (Donkó & Nyíri 2000; Daligault 2006a). We find

$$v_{\text{sed}} \gtrsim 3 \times 10^{-7} \rho_9^{-0.6} \left( \frac{T_8}{3} \right)^{0.3} \left( \frac{\Delta Y_e/Y_e}{0.01} \right) N_s^{2/3} \text{ cm/s}. \quad (5)$$

Comparing with the accretion velocity  $v_{\text{accr}} = \dot{m}/\rho = 10^{-5} \dot{m}_4 \rho_9^{-1} \text{ cm/s}$ , we find that the critical cluster size above which the particles sediment out is

$$N_{s,\text{crit}} = 200 \rho_9^{-0.6} \left( \frac{T_8}{3} \right)^{-0.45} \dot{m}_4^{3/2} \left( \frac{\Delta Y_e/Y_e}{0.01} \right)^{-3/2}. \quad (6)$$

Note that the simple nature of our estimates means that there are considerable uncertainties in the crystallization and sedimentation velocities we find here. Despite this, however, the timescale for a cluster to grow to a size  $N_{s,\text{crit}}$  is so short that the conclusion that the solid particles rapidly fall out of the ocean seems inescapable.

Setting  $N_{s,\text{crit}} = 1$  in Eq. (6) provides an estimate of when relative separation of light and heavy elements (without forming solid clusters) is expected to occur. This gives  $\dot{m} = 300 \text{ g cm}^{-2} \text{ s}^{-1} \approx 0.003 \dot{m}_{\text{Edd}}$ , below the accretion rates of persistent LMXBs or most transient LMXBs in outburst. However, separation of light and heavy elements is something that should be considered during quiescent periods in transient accretors (Brown et al. 2002) or at low accretion rates (Peng, Brown, & Truran 2007).

### 2.3. Compositional buoyancy and convection

After the solid particles form and sediment out, the fluid left behind is lighter than the fluid immediately above it and so will have a tendency to buoyantly rise. This is counteracted by the thermal profile, which is stably stratified in the absence of a composition gradient such that a rising fluid element will be colder than its surroundings and will tend to sink back down. A measure of the buoyancy is the convective discriminant  $\mathcal{A}$ , which is related to the Brunt-Väisälä frequency  $N^2 = -g\mathcal{A}$  (Cox 1980). For a two-component mixture in the ocean, we can write (Bildsten & Cumming 1998)

$$\mathcal{A}H_P = \frac{\chi_T}{\chi_\rho} (\nabla - \nabla_{\text{ad}}) + \frac{\chi_X}{\chi_\rho} \nabla_X; \quad (7)$$

here,  $X$  is the mass fraction of the lighter element (Fe or O in the examples above),  $\chi_X = \partial \ln P / \partial \ln X|_{T,\rho}$ ,  $\chi_\rho = \partial \ln P / \partial \ln \rho|_{X,T}$ ,  $\chi_T = \partial \ln P / \partial \ln T|_{X,\rho}$ , and the temperature and composition gradients are  $\nabla = -H_P(d \ln T / dr)$  and  $\nabla_X = -H_P(d \ln X / dr)$ . The adiabatic gradient is taken at constant entropy  $S$  and composition:  $\nabla_{\text{ad}} = -H_P(d \ln T / dr|_{S,X})$ . Note that  $\chi_X$ ,  $\chi_T$ , and  $\chi_\rho$  are all positive quantities. If  $\mathcal{A} < 0$  or  $N^2 > 0$  the ocean is stable to convection. For example, if the composition is uniform so that  $\nabla_X = 0$ , stability to convection requires the familiar condition  $\nabla < \nabla_{\text{ad}}$ . Only one term describing the variation of the composition is needed in Eq. (7) since we consider a two-component mixture. We generalize to more than two species in the next section.

In steady state the composition profile is lighter with increasing depth:  $\nabla_X > 0$ . Such a profile will not lead to convection as long as the gradient is small enough that the destabilizing effect of the composition profile is compensated by the thermal buoyancy represented by the first term in Eq. (7). The maximum stable composition gradient is

$$\nabla_{X,\text{max}} = \frac{\chi_T}{\chi_X} (\nabla_{\text{ad}} - \nabla) \approx \frac{\chi_T \nabla_{\text{ad}}}{\chi_X}, \quad (8)$$

where we assume that the large thermal conductivity in the ocean due to the degenerate electrons results in an almost isothermal profile  $\nabla \ll \nabla_{\text{ad}}$  (see §4).

As accretion continues, light elements are continually deposited at the base of the ocean and must be transported upwards by convection. We expect therefore that the composition gradient will adjust to be close to but slight greater than  $\nabla_{X,\text{max}}$  so as to result in the required convective flux of composition  $F_X = \dot{m}(X_0 - X_b)$ , where  $X_0$  is the incoming composition and  $X_b$  is the composition at the base of the ocean (that results in freezing of solid with mass fraction  $X_0$ ).

We can estimate  $\nabla_X - \nabla_{X,\text{max}}$  in steady state and the corresponding convective velocity using mixing length theory. The acceleration of a fluid element is  $g\mathcal{A}$ , giving a convective velocity

$$v_{\text{conv}}^2 \sim gl_m^2 \frac{\chi_X \nabla_X - \chi_T \nabla_{\text{ad}}}{H_P \chi_\rho}, \quad (9)$$

where  $l_m$  is the mixing length and we again assume  $\nabla = 0$  for simplicity. After moving a distance  $l_m$ , the mass fraction differs from its surroundings by an amount  $(l_m/H_P)X\nabla_X$ , implying that there is a flux of composi-

tion

$$F_X \sim \rho v_{\text{conv}} \frac{l_m X \nabla_X}{H_P}. \quad (10)$$

Setting this equal to the steady state flux at the base of the ocean  $F_X = \dot{m}(X_0 - X_b) = \rho v_{\text{accr}}(X_0 - X_b)$  gives the maximum convective velocity

$$\begin{aligned} v_{\text{conv}} &\sim v_{\text{accr}} \left( \frac{H_P}{l_m} \right) \frac{X_0 - X_b}{X_b \nabla_{X,\text{max}}} \\ &\sim v_{\text{accr}} \left( \frac{H_P}{l_m} \right) \left( \frac{X_0 - X_b}{X_b} \right) \nabla_{\text{ad}}^{-1} \frac{\chi_X}{\chi_T}. \end{aligned} \quad (11)$$

In the deep ocean where pressure is dominated by degenerate electrons, all factors on the right hand side of Eq. (11) are of order unity except for  $\chi_X \approx \chi_\rho(1 - Y_{\text{Se}}/Y_e) \sim 0.1$ , where  $Y_{\text{Se}} = 34/79$ ; and  $\chi_T \approx (T/P_e)(\partial P_i / \partial T) \sim 10k_B T / [ \langle Z \rangle E_F ]$  (e.g., Hansen & Kawaler 1994), where  $P_e$  is the electron pressure,  $P_i$  the ion pressure, and  $E_F$  is the Fermi energy excluding rest mass. For an ocean temperature of  $3 \times 10^8$  K and  $E_F = 5.1\rho_9^{1/3}Y_e^{1/3}$  MeV (the electrons are relativistic),  $\chi_T \sim 0.001$ . Therefore,  $v_{\text{conv}}$  is about two orders of magnitude larger than the accretion velocity. Given that chemical separation is being driven by accretion, it may be surprising that  $v_{\text{conv}}$  is much larger than  $v_{\text{accr}}$ . The reason is that only a very shallow composition gradient can be tolerated in the deep ocean where  $k_B T \ll E_F$ , requiring  $v_{\text{conv}} \gg v_{\text{accr}}$  to transport the required flux of composition.

Comparing Eqs. (9) and (11), we see that  $\nabla_X - \nabla_{X,\text{max}} \lesssim (v_{\text{accr}}/c_s)^2 [\chi_\rho \chi_X (X_0 - X_b)^2 / \nabla_{\text{ad}}^2 \chi_T^2 X_b^2] \ll 1$ , where  $c_s = (gH_P)^{1/2}$  is the sound speed. In other words the convective velocities needed to transport the flux of light elements through the ocean are very subsonic, implying the composition gradient is extremely close to the marginally stable gradient  $\nabla_X \approx \nabla_{X,\text{max}}$ . This is analogous to efficient convective heat transport for which  $\nabla \approx \nabla_{\text{ad}}$ .

Another piece of physics that could potentially play a role is diffusion. Inwards diffusion of composition will occur down the composition gradient  $\nabla_X$ , and in principle if efficient enough could mediate the need for convection. The diffusive flux is much smaller than the convective flux, however. To see this, we use Eq. (3) for a selenium OCP:

$$D = 2 \times 10^{-6} \rho_9^{-1} \left( \frac{T_8}{3} \right)^{2.5} \text{ cm}^2/\text{s}. \quad (12)$$

The diffusion time across a composition scale height  $l_X = H_P / \nabla_X$ , where the pressure scale height  $H_P = 1900 \rho_9^{1/3} (Y_e / 0.43)^{4/3} (g_{14} / 2.45)^{-1}$  cm is

$$t_D = \frac{l_X^2}{D} = 5 \times 10^4 \nabla_X^{-2} \rho_9^{1.3} \left( \frac{T_8}{3} \right)^{-2.5} \text{ yrs}. \quad (13)$$

This is much longer than the accretion timescale given by Eq. (2), or the convective turnover time given by

$$t_{\text{conv}} = l_m / v_{\text{conv}} \sim 100 l_m / v_{\text{accr}}, \quad (14)$$

implying that microscopic diffusion does not play a significant role in transporting light elements across the ocean.

We also note that our conclusion that the ocean is convectively unstable depends on the slope of the liquidus

curve in the phase diagram. In all of the cases we have considered, the composition profile that would exist if the ocean followed the liquidus curve as fluid elements move to higher pressure is too steep to be maintained by thermal buoyancy. If this were not the case, a different picture would result: the composition in the ocean at a given pressure would correspond to the composition of the liquidus curve at each depth, and a steady hail of solid particles would fall through the ocean to the solid crust at the base. Given the phase diagrams for two- and three-component plasmas we have calculated, however, this situation appears not to arise.

We therefore expect that the ocean adjusts its composition from  $X_0$  at the top to  $X_b$  at the base with a mixing zone in which the gradient is  $\nabla_X \approx \nabla_{X,\max}$ . Because this gradient is very shallow in the deep degenerate part of the ocean ( $\nabla_{X,\max} \sim 10k_B T / [Z]E_F$ ), we expect the mixing zone to have substantial thickness. We investigate this in the next section with detailed models of the steady-state ocean, and find that the entire ocean is expected to undergo mixing all the way up to the layer of light elements that supplies the ocean with new material through nuclear burning. The shallow gradient also means that there is a nearly uniform composition throughout the bulk of the ocean, which is set by the phase diagram at the freezing point.

### 3. ILLUSTRATIVE MODELS OF A CONVECTIVE OCEAN

In §2 we argued that crystallization and sedimentation would drive a convective instability at the base of the ocean. We now calculate detailed but illustrative models of the steady-state ocean based on this picture. We use mixing length theory to calculate the convective velocity, keeping the mixing length as a free parameter; whether mixing length theory is appropriate for compositionally-driven convection is an open question. As we discuss further in §5, we also neglect other hydrodynamical circulations (e.g. Eddington-Sweet circulation driven by rotation), the effects of rotation or magnetic fields on the convection itself, or other transport mechanisms such as turbulent mixing that could lead to transport of composition through the ocean.

We first allow the ocean to extend to arbitrarily low density; i.e., we first neglect the light element layer which overlies the ocean (§3.1) and then show how the light element layer can be incorporated self-consistently into a steady-state model of the ocean (§3.2). The models in §3.1 and §3.2 are isothermal; in §4 we consider the effect of the mixing on the thermal profile.

#### 3.1. A first model of the ocean

We first calculate the steady state in the ocean for the case where nuclear reactions are unimportant in the convection zone. We show results for the specific two-component mixtures discussed in §2, but for generality we keep the number of species arbitrary in the derivations that follow. The continuity equation for the flow of species  $i$  is

$$\frac{dX_i}{dt} + \mathbf{v}_{\text{accr}} \cdot \nabla X_i = -\frac{1}{\rho} \nabla \cdot (\rho \mathbf{v}_{\text{conv}} D X_i), \quad (15)$$

where

$$D X_i = \frac{\xi}{2} X_i \nabla X_i \quad (16)$$

for an inward-convecting blob, and the convective velocity from mixing length theory is given by (e.g., Kippenhahn & Weigert 1994)

$$v_{\text{conv}}^2 = \xi^2 \frac{g H_P}{8 \chi_\rho} \left( \chi_T (\nabla - \nabla_{\text{ad}}) + \sum_{i=1}^{n-1} \chi_{X_i} \nabla X_i \right), \quad (17)$$

where  $n$  is the total number of chemical species in the ocean,  $X_i$  is the mass fraction of species  $i$ , and the parameter  $\xi = l_m / H_P$  is the ratio between the convection mixing length  $l_m$  and the scale height. In mixing length theory the value of  $\xi$  is highly uncertain; we assume that  $\xi = 1$  in this paper, but  $\xi$  could be an order of magnitude or two smaller than this.

In steady state and for vertical flow in plane-parallel geometry (a good assumption since the ocean is thin compared to the stellar radius), we have

$$v_{\text{accr}} \frac{dX_i}{dr} = \frac{\xi}{2\rho} \frac{d}{dr} (\rho v_{\text{conv}} X_i \nabla X_i). \quad (18)$$

Integrating from the top of the ocean to some depth within the ocean, using the fact that  $\rho v_{\text{accr}} = \dot{m}$  is a constant, we find

$$v_{\text{accr}} (X_i - X_{i,0}) = v_{\text{conv}} \frac{\xi}{2} X_i \nabla X_i. \quad (19)$$

Note that at the top of the convection zone, when  $v_{\text{conv}} = 0$ , we have  $X_i = X_{i,0}$  for each  $X_i$ . Rewriting Eq. (19) gives

$$\frac{dX_i}{d \ln P} = \frac{v_{\text{accr}}}{v_{\text{conv}}} \frac{2}{\xi} (X_i - X_{i,0}) \quad (20)$$

which can be integrated for each species  $i = 1, 2, \dots, n-1$  (the composition of species  $n$  follows from the constraint  $\sum_{i=1}^n X_i = 1$ ).

The  $n-1$  differential equations (20) are coupled because the convective velocity depends on a sum over all species. To obtain an expression for the convective velocity, we multiply Eq. (19) by  $\chi_{X_i}$  and sum over species to obtain

$$\sum_{i=1}^{n-1} \chi_{X_i} \nabla X_i = \frac{v_{\text{accr}}}{v_{\text{conv}}} \frac{2}{\xi} \sum_{i=1}^{n-1} \chi_{X_i} \frac{X_i - X_{i,0}}{X_i}. \quad (21)$$

We argued in §2 that small convective velocities  $v_{\text{conv}} \ll c_s$  are required to transport the composition flux. Therefore,

$$\sum_{i=1}^{n-1} \chi_{X_i} \nabla X_i \approx \chi_T (\nabla_{\text{ad}} - \nabla) \quad (22)$$

[cf. Eq. (8)], and we can replace the left-hand side of Eq. (21) with  $\chi_T (\nabla_{\text{ad}} - \nabla)$ . Rearranging, we find an expression for  $v_{\text{conv}}$ :

$$v_{\text{conv}} = v_{\text{accr}} \frac{2}{\xi} \frac{1}{\chi_T (\nabla_{\text{ad}} - \nabla)} \sum_{i=1}^{n-1} \chi_{X_i} \frac{X_i - X_{i,0}}{X_i}. \quad (23)$$

As a check we see that for two species ( $n = 2$ ), Eqs. (20) and (23) give  $d \ln X / d \ln P = (\chi_T / \chi_X) (\nabla_{\text{ad}} - \nabla)$  which is the marginally stable composition gradient (§2.3).

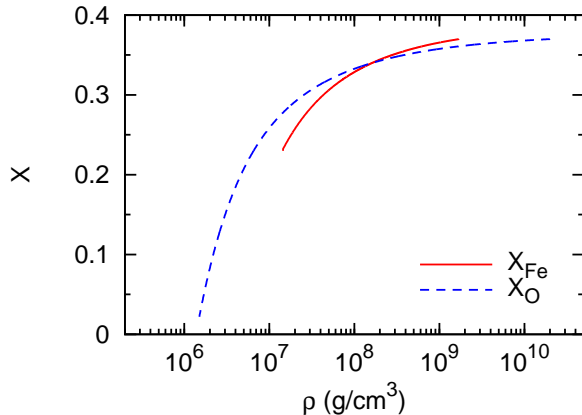


FIG. 2.— (Color online) The composition profile in the convection zone of a  $T = 3 \times 10^8$  K ocean composed of  $^{56}\text{Fe}$ ,  $^{79}\text{Se}$  (solid line) and  $^{16}\text{O}$ ,  $^{79}\text{Se}$  (dashed line). The hydrogen/helium burning layer is neglected.

To obtain a solution, the location and composition of the base of the ocean are specified, and then Eq. (20) is integrated outward for each  $X_i$ . The top of the convection zone is located at the point where the composition matches the incoming composition,  $X_i = X_{i,0}$ . In Fig. 2 we present our results for the  $^{56}\text{Fe}$ - $^{79}\text{Se}$  and  $^{16}\text{O}$ - $^{79}\text{Se}$  systems described in §2. The ocean temperature is taken to be  $T = 3 \times 10^8$  K. To calculate the various  $\nabla$ 's and  $\chi$ 's, we assume that the electron pressure is given by the fitting formula of Paczyński (1983), and following Paper I we include Coulomb corrections for the ions using the free energy from DeWitt & Slattery (2003). Note that the equations used in this section to calculate the composition profile are all independent of  $\xi$ ; only the convective velocity depends on this value. Therefore, the potentially large error introduced by our choice of  $\xi$  does not affect our results.

The solutions show the expected behavior, that at large depths where  $k_B T \ll E_F$ , the composition gradient is very shallow, but as the integration continues further upwards, the gradient steepens as  $E_F$  drops. In each case, the ocean is substantially enriched in light elements throughout most of its mass. Figure 3 compares the convective velocity with the accretion velocity for these two cases, assuming  $\xi = 1$  and  $\dot{m}_4 = 3$  (i.e., an accretion rate of  $0.3\dot{m}_{\text{Edd}}$ ). Towards the top of the ocean, where the composition gradient becomes significant ( $E_F$  becomes comparable to  $k_B T$ ), the convective velocity drops towards the accretion velocity.

### 3.2. Including nuclear burning of light elements

Figure 2 shows that in the oxygen-selenium two-species model at  $T = 3 \times 10^8$  K, the convection zone extends into the hydrogen/helium burning layer ( $\rho \sim 10^5$ – $10^7$  g/cm $^3$ ). This effect becomes more pronounced at lower temperatures, as might be expected when  $\dot{m} < 0.3\dot{m}_{\text{Edd}}$ : empirically the density at the top of the convection zone goes as  $T^{2.3}$  for typical ocean temperatures, in both the O-Se and the Fe-Se models. Therefore, an accurate model of the entire convection zone must include the effects of nuclear reactions. As a first approximation, we use

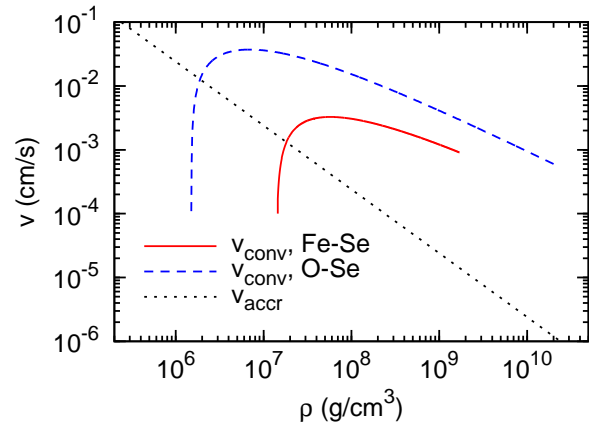


FIG. 3.— (Color online) The accretion velocity for  $\dot{m} = 3 \times 10^4$  g cm $^{-2}$  s $^{-1}$ , and the convective velocity within the convection zone of a  $T = 3 \times 10^8$  K ocean composed of  $^{56}\text{Fe}$ ,  $^{79}\text{Se}$  (solid line) and  $^{16}\text{O}$ ,  $^{79}\text{Se}$  (dashed line).

the following simplified model for the burning layer: At  $\rho = 10^4$  g/cm $^3$  the neutron star is composed only of hydrogen and helium, with  $X_{\text{H}} = 0.7$  and  $X_{\text{He}} = 0.3$ . The relative abundance of hydrogen and helium is maintained as these elements undergo nuclear reactions and convective mixing, such that  $X_{\text{H}}/X_{\text{He}} = 0.7/0.3$  is a constant throughout the ocean. This mixture burns at the triple-alpha rate (Hansen & Kawaler 1994)

$$R_{3\alpha} \approx 10^{-6} \left( \frac{\rho}{\text{g/cm}^3} \right)^2 (0.3X_1)^2 \frac{e^{-44/T_8}}{T_8^3} \text{ s}^{-1}, \quad (24)$$

where  $X_1$  is the mass fraction of the H/He composite with  $X_{\text{H}} = 0.7X_1$  and  $X_{\text{He}} = 0.3X_1$ . Each gram of the mixture burns to  $X_i^{\text{burn}}$  grams of each chemical species  $i > 1$  (so that  $\sum_{i=2}^n X_i^{\text{burn}} = 1$ ).

We use this model for the burning layer to calculate the steady state in the ocean for the case where nuclear reactions are important in the convection zone. The continuity equation for each species becomes

$$\frac{dX_1}{dt} + \mathbf{v}_{\text{accr}} \cdot \nabla X_1 = -\frac{1}{\rho} \nabla \cdot (\rho \mathbf{v}_{\text{conv}} D X_1) - X_1 R_{3\alpha} \quad (25)$$

for  $i = 1$  and

$$\frac{dX_i}{dt} + \mathbf{v}_{\text{accr}} \cdot \nabla X_i = -\frac{1}{\rho} \nabla \cdot (\rho \mathbf{v}_{\text{conv}} D X_i) + X_i^{\text{burn}} X_1 R_{3\alpha} \quad (26)$$

for  $i = 2, 3, \dots, n$ . In steady state we have

$$v_{\text{accr}} \frac{dX_1}{dr} = \frac{\xi}{2\rho} \frac{d}{dr} (\rho v_{\text{conv}} X_1 \nabla X_1) + X_1 R_{3\alpha} \quad (27)$$

and

$$v_{\text{accr}} \frac{dX_i}{dr} = \frac{\xi}{2\rho} \frac{d}{dr} (\rho v_{\text{conv}} X_i \nabla X_i) - X_i^{\text{burn}} X_1 R_{3\alpha}. \quad (28)$$

Above the convection zone (where  $v_{\text{conv}} = 0$ ) we use

$$v_{\text{accr}} \frac{dX_1}{d \ln P} = -X_1 R_{3\alpha} H_P \quad (29)$$

to solve for  $X_1$  as a function of  $P$ , and then

$$v_{\text{accr}} \frac{dX_i}{d \ln P} = X_i^{\text{burn}} X_1 R_{3\alpha} H_P \quad (30)$$

or

$$X_i = (1 - X_1) X_i^{\text{burn}} \quad (31)$$

to find the  $X_i$ ,  $i > 1$  values. These equations are solved inward from  $\rho = 10^4 \text{ g/cm}^3$ , where we set  $X_1 = 1$  and  $X_i = 0$  for  $i > 1$ . Within the convection zone we use the following method to find the  $X_i$ 's: We first specify the location of the top of the convection zone,  $P_0$ . The  $X_{i,0}$  values used in the equations below are then found by solving Eqs. (29) and (31) down to this point. The value of  $P_0$  is not known a priori, so the  $X_i$ 's are found for a given  $P_0$  and then the value is varied until the composition changes smoothly across the convection zone boundary. We define a new variable,  $W$ , such that

$$\frac{dW}{dr} = \frac{X_1 R_{3\alpha}}{v_{\text{accr}}} \quad (32)$$

and  $W = 0$  at the top of the convection zone (when  $X_i = X_{i,0}$ ). Then the equation for the convective velocity is

$$\begin{aligned} \sum_{i=1}^{n-1} \chi_{X_i} \frac{X_i - X_{i,0}}{X_i} - W \left( \frac{\chi_{X_1}}{X_1} - \sum_{i=2}^{n-1} \frac{\chi_{X_i}}{X_i} X_i^{\text{burn}} \right) \\ = \frac{v_{\text{conv}}}{v_{\text{accr}}} \frac{\xi}{2} \sum_{i=1}^{n-1} \chi_{X_i} \nabla_{X_i}, \end{aligned} \quad (33)$$

or

$$v_{\text{conv}} = v_{\text{accr}} \frac{2}{\xi} \frac{1}{\chi_T (\nabla_{\text{ad}} - \nabla)} \left[ \sum_{i=1}^{n-1} \chi_{X_i} \frac{X_i - X_{i,0}}{X_i} - W \left( \frac{\chi_{X_1}}{X_1} - \sum_{i=2}^{n-1} \frac{\chi_{X_i}}{X_i} X_i^{\text{burn}} \right) \right]. \quad (34)$$

The  $n$  coupled differential equations to solve are

$$\frac{dX_1}{d \ln P} = \frac{v_{\text{accr}}}{v_{\text{conv}}} \frac{2}{\xi} (X_1 - X_{1,0} - W); \quad (35)$$

$$\frac{dX_i}{d \ln P} = \frac{v_{\text{accr}}}{v_{\text{conv}}} \frac{2}{\xi} (X_i - X_{i,0} - W X_i^{\text{burn}}), \quad (36)$$

for  $i = 2, 3, \dots, n-1$ ; and Eq. (32). We solve these equations through iteration, first guessing the  $X_i$  values at every point in the convection zone, then using these values to find  $W$ , and so on, until convergence is reached.

In Fig. 4 we present our results for the  $^{56}\text{Fe}$ - $^{79}\text{Se}$  and  $^{16}\text{O}$ - $^{79}\text{Se}$  systems discussed in §2; again we choose  $m_4 = 3$ ,  $\xi = 1$ , and an ocean temperature  $T = 3 \times 10^8 \text{ K}$ . For comparison we also present the  $X_{\text{Fe}}$ ,  $X_{\text{O}}$ , and  $X_{\text{Se}}$  profiles when the hydrogen/helium burning layer is neglected (§3.1). These profiles are nearly the same as the profiles when the burning layer is included, except at the top of the convection zone where the latter profiles are very steep. The change in the slope of the profiles from §3.1 to §3.2 can be understood from Eq. (22): This equation states that within the convection zone  $\sum_{i=1}^{n-1} \chi_{X_i} \nabla_{X_i}$  follow the adiabatic gradient, but places no such restriction on the individual  $X$  profiles. Therefore, at the top of the convection zone, the Fe, O, and Se

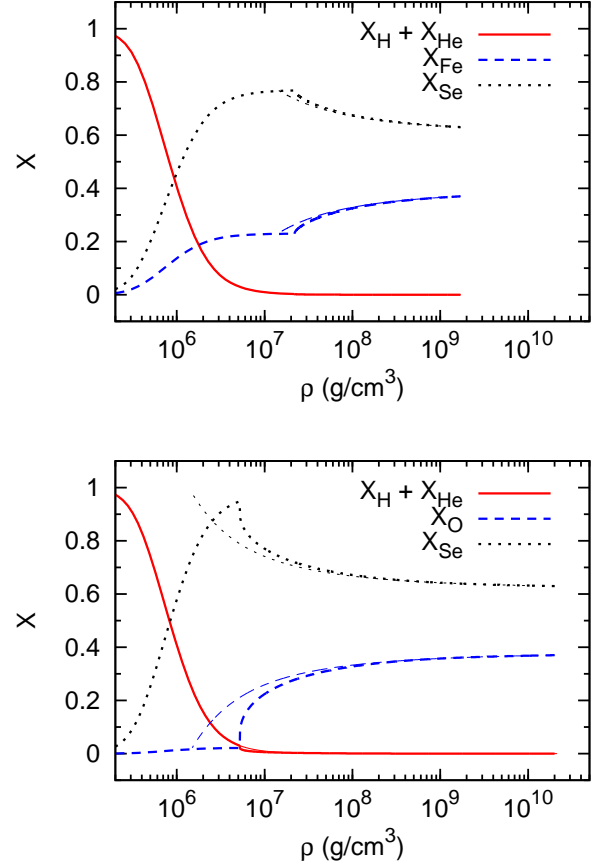


FIG. 4.— (Color online) The composition profile within and directly above the convection zone of a  $T = 3 \times 10^8 \text{ K}$  ocean composed of  $^{56}\text{Fe}$ ,  $^{79}\text{Se}$  (top panel) and  $^{16}\text{O}$ ,  $^{79}\text{Se}$  (bottom panel). A layer of hydrogen and helium is placed on top of the ocean and nuclear reactions are crudely modeled. For comparison the  $X_{\text{Fe}}$ ,  $X_{\text{O}}$ , and  $X_{\text{Se}}$  profiles when the burning layer is neglected (Fig. 2), and the  $X_{\text{H}} + X_{\text{He}}$  profiles when convection is turned off [Eqs. (29) and (31)] are also plotted, as thin lines with the same patterns as the profiles from the full calculation. The convection zone begins at the point where the two  $X_{\text{H}} + X_{\text{He}}$  curves diverge, at a density of  $7.2 \times 10^6 \text{ g/cm}^3$  for the F-Se system and  $2.6 \times 10^6 \text{ g/cm}^3$  for the O-Se system.

composition profiles rise sharply with increasing density because of the correspondingly large drop in the H-He profile. The burning layer acts as a barrier to convection, such that the convection zone ends abruptly at the base of this layer.

Finally, in Fig. 4 we present  $X_{\text{H}} + X_{\text{He}}$  profiles when convection is ignored [such that Eqs. (29) and (31) apply across the entire ocean]. The shape of these profiles results from the balance between accretion driving the H-He mixture deeper and nuclear reactions converting H-He into heavier elements as it travels inward; the profiles can be estimated using Eqs. (2) and (24):  $1 - t_{\text{accr}} R_{3\alpha} \simeq X_1 \Rightarrow X_1 \propto \rho^{5/3}$  for  $X_1 \lesssim 0.1$ . In addition to the sharp drop at the top of the convection zone, the profiles when convection is included differ in that they fall more slowly with increasing density, due to their larger inward velocity; since  $v_{\text{conv}} \propto \rho^{-2/3}$  in the deep ocean,  $X_1 \propto \rho^{3/2}$  for  $X_1 \lesssim 10^{-3}$ . The  $X_{\text{H}} + X_{\text{He}}$  profiles there-

fore cross at some depth in the ocean; i.e., convection causes some hydrogen-helium to mix into deeper layers. While this mixing will change the amount of burning at each depth in the convection zone, we do not expect the thermal profile in this region to change, because the amount of helium in the convection region is very small (less than 10% by mass of the total helium in the star, and less than 1% of the total mass at any depth in the convection zone; see Fig. 4).

#### 4. EFFECT OF MIXING ON THE THERMAL PROFILE

So far we have taken the ocean to be isothermal, which is a good first approximation for the bulk of the ocean where thermal conductivity efficiently transports heat (Bildsten & Cutler 1995). In this section, we discuss the effect of convective mixing on the thermal profile and evaluate the heating associated with the transport of light elements upwards through the ocean and the steady-state thermal profile.

When mixing is unimportant, the main contribution to the heat flux in the ocean comes from energy released by nuclear reactions in the crust. These reactions release an energy of  $\approx 1.7$  MeV per nucleon (e.g., Haensel & Zdunik 2008), of which  $Q_b \sim 0.1$ – $1$  MeV per nucleon flows outward through the ocean, depending on the accretion rate (Brown 2000). This component of the heat flux can be written as

$$F_{\text{crust}} = Q_b \frac{\dot{m}}{m_p}. \quad (37)$$

The temperature gradient required to carry the heat flux is given by

$$\nabla = \frac{FH_P}{KT}, \quad (38)$$

where

$$K = \frac{4ac}{3\rho\kappa_{\text{rad}}} + K_{\text{cd}} \quad (39)$$

is the total thermal conductivity including both radiation and conduction contributions,  $a$  is the radiation constant,  $c$  is the speed of light,  $\kappa_{\text{rad}}$  is the radiative opacity (e.g., Schatz et al. 1999),  $K_{\text{cd}} = n_e k_B^2 T / (m_* \nu_c)$  is the thermal conductivity,  $m_* = m_e + E_F / c^2$  is the effective mass of the electrons, and  $\nu_c$  is the collision frequency. In the ocean, the relevant collision frequency is that between electrons and ions:  $\nu_c = 4e^4 m_* \Lambda / (3\pi \hbar^3) \langle Z^2 \rangle / \langle Z \rangle$ , where  $\Lambda$  is the Coulomb logarithm (Yakovlev & Urpin 1980; Schatz et al. 1999). For densities  $\rho \gtrsim 10^7$  g/cm<sup>3</sup> the electrons are degenerate and relativistic, and the contribution of radiation to  $K$  is negligible; in this case we find

$$\nabla \simeq 0.03 \dot{m}_4 \left( \frac{Q_b}{0.1 \text{ MeV}} \right) \left( \frac{T_8}{3} \right)^{-2} \times \left( \frac{\langle Z^2 \rangle / \langle Z \rangle}{30} \right) \left( \frac{g_{14}}{2.45} \right)^{-1}, \quad (40)$$

where in the above we have set  $\Lambda = 1$ . We see therefore that over most of the ocean a shallow temperature gradient is sufficient to conduct the heat flux from the crust, and in particular  $\nabla \ll \nabla_{\text{ad}} \sim 0.35$  as we assumed in §3. Note that this is not true for  $\rho \lesssim 10^7$  g/cm<sup>3</sup>, where the

electrons are nonrelativistic. In that regime  $HP/K_{\text{cd}} \propto \rho^{-1/3}$ , such that at low densities  $HP/K_{\text{cd}} > \nabla_{\text{ad}}$ . The radiation contribution to the total  $K$  becomes important at these densities, partially offsetting the effect of a low  $K_{\text{cd}}$ . Nevertheless, under certain conditions (e.g.,  $\dot{m} \geq \dot{m}_{\text{Edd}}$  and  $T < 10^9$  K)  $\nabla > \nabla_{\text{ad}}$  at the top of the ocean. It is unclear what happens in that case; a complete understanding may require a time-dependent calculation (see §5).

Thermal conduction also readily conducts the latent heat away from the ocean floor. We can estimate the latent heat release using the equations from Paper I for the free energies of the liquid and solid states [e.g., equations (23) and (24) of that paper]; the latent heat released on freezing is of order  $k_B T / \langle A \rangle \approx 0.1 T_8 [60 / \langle A \rangle]$  keV per nucleon. Much smaller than  $Q_b$ , the latent heat is removed with only a small temperature gradient. This contrasts with, e.g., freezing of solid material in the Earth's core, in which the temperature gradient required to conduct the latent heat away is  $\nabla > \nabla_{\text{ad}}$ , so that the latent heat release drives thermal convection (Stevenson 1981).

When chemical separation drives convection in the ocean, we must also consider the convective heat flux in addition to the conductive heat flux. In mixing length theory the heat flux is

$$\mathbf{F}_{\text{conv}} = \frac{\xi}{2} \rho \mathbf{v}_{\text{conv}} c_P T (\nabla - \nabla_{\text{ad}}), \quad (41)$$

where  $c_P$  is the heat capacity. Using Eq. (23) for the convective velocity together with the fact that  $\rho v_{\text{accr}} = \dot{m}$ , we find

$$\mathbf{F}_{\text{conv}} = -F_{\text{conv}} \hat{r} \quad (42)$$

with

$$F_{\text{conv}} = \frac{c_P T \dot{m}}{\chi_T} \sum_{i=1}^{n-1} \chi_{X_i} \frac{X_i - X_{i,0}}{X_i}. \quad (43)$$

Here  $\hat{r}$  is the radial unit vector. Note that  $F_{\text{conv}} > 0$  so that the convection transports heat inwards. This is because, unlike thermally-driven convection,  $\nabla < \nabla_{\text{ad}}$  so that a fluid element displaced adiabatically outwards is cooler than its surroundings at its new location.

We show the convective flux as  $F_{\text{conv}} m_p / \dot{m}$  with  $\dot{m} = 3 \times 10^4$  g cm<sup>-2</sup> s<sup>-1</sup> in Fig. 5. In the ocean, the heat capacity is set by the ions; using the internal energy expansion from DeWitt & Slattery (2003) we find  $c_P \sim (1-4) k_B / [\langle A \rangle m_p]$  giving  $c_P T / m_p \sim (0.1-0.6) T_8 [60 / \langle A \rangle]$  keV per nucleon, where the range of values is across the depth of the ocean. Although  $c_P T / m_p$  is much smaller than  $Q_b$ , the convective flux has an additional factor of  $\chi_X / \chi_T \propto E_F / (k_B T)$ . This gives an extra factor of 10–100, so that the final convective flux is  $\sim 10^{-2}$ – $10^{-1}$  MeV per nucleon, which can be comparable to  $Q_b$ . For the O-Fe ocean in Fig. 5, the convective flux is  $\approx 0.2$  MeV per nucleon at the base of the convection zone. For Fe-Se, the smaller contrast between the heavy and light elements gives a much smaller flux. For two species, the composition flux is  $F_X = \dot{m}(X - X_0)$ , so that we can write  $F_{\text{conv}} = F_X c_P T \chi_X / (X \chi_T) = F_X c_P (\partial \ln T / \partial \ln X |_{P,\rho})$ . The convective heat flux corresponds to the rate of change of internal energy given the flux of composition at each depth [compare equation (2) of Montgomery et al. 1999].

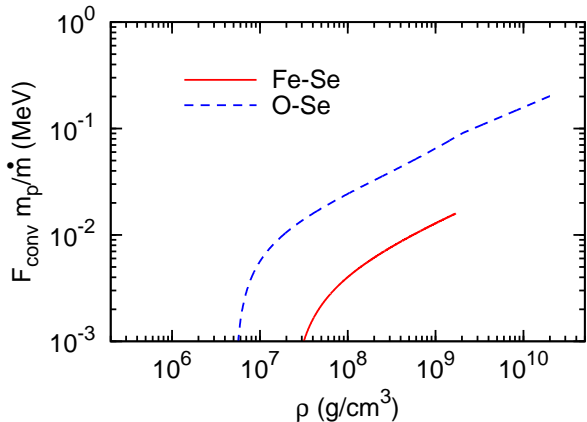


FIG. 5.— (Color online) The convective flux for a  $\dot{m} = 3 \times 10^4 \text{ g cm}^{-2} \text{ s}^{-1}$ ,  $T = 3 \times 10^8 \text{ K}$  ocean composed of  $^{56}\text{Fe}$ ,  $^{79}\text{Se}$  (solid line) and  $^{16}\text{O}$ ,  $^{79}\text{Se}$  (dashed line).

Figure 5 shows that the inwards convective flux increases with depth in the ocean  $dF_{\text{conv}}/dy > 0$ . This implies that there is a local cooling at each depth in the ocean, and so while it is a good approximation to assume the ocean is isothermal when calculating the convective velocity and composition profile of the mixed zone, in fact the isothermal models we presented in §3 are not in a thermal steady-state. To see what the thermal steady-state must look like, we write down the entropy equation

$$T \frac{Ds}{Dt} = \frac{dF}{dy} + \epsilon, \quad (44)$$

where  $s$  is the specific entropy,  $\epsilon$  is the sum of all sources and sinks of heat (latent heat release, nuclear reactions, neutrino cooling, etc.), and  $D/Dt = d/dt + \dot{m}dy/dy$  is the total derivative for a fluid element. The heat flux  $F$  is the sum of convective and conductive heat fluxes. In steady state ( $ds/dt = 0$ ) the left hand side of Eq. (44) is given by (e.g., Brown & Bildsten 1998)

$$T \frac{Ds}{Dt} = \frac{c_P T \dot{m}}{y} \left( \nabla - \nabla_{\text{ad}} + \frac{1}{\chi T} \sum_{i=1}^{n-1} \chi_{X_i} \nabla_{X_i} \right), \quad (45)$$

much smaller than the  $dF/dy$  terms on the right hand side since in the convective region  $\sum_{i=1}^{n-1} \chi_{X_i} \nabla_{X_i} \approx \chi T (\nabla_{\text{ad}} - \nabla)$  [Eq. (22)] (the convection zone is very close to adiabatic). Neglecting any contributions to  $\epsilon$  in the ocean, e.g. nuclear reactions or the small latent heat release at the boundary, we must have  $dF/dy = 0$  in steady state, or an outwards conductive flux  $F_{\text{cond}} = F_{\text{crust}} + F_{\text{conv}}$ . The picture we arrive at is that starting with an isothermal ocean, the inwards convection of heat steepens the temperature gradient until the outwards conductive flux balances the convective flux.

We see therefore that the effect of the mixing is to add a contribution to the conductive flux in the deep ocean of as much as 0.2 MeV per nucleon for an O-Se mixture. At high accretion rates  $\dot{m} \gtrsim 0.1 \dot{m}_{\text{Edd}}$ , this is comparable to or larger than the flux from the crust  $Q_b \sim 0.1 \text{ MeV}$  per nucleon (Brown 2000; at lower accretion rates  $\dot{m} \sim 0.01 \dot{m}_{\text{Edd}}$ , a larger fraction of the heat released in the crust flows outwards, and  $Q_b \sim 1 \text{ MeV}$ ). We show in

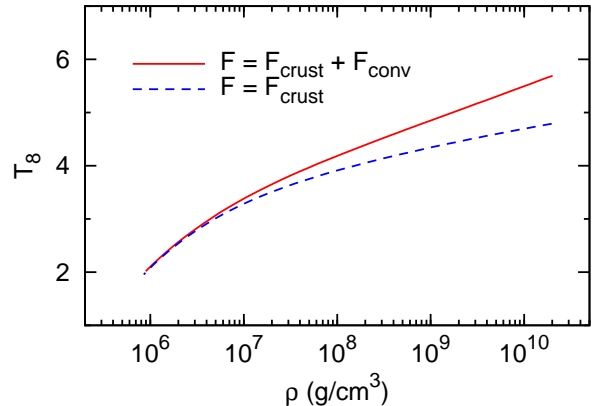


FIG. 6.— (Color online) The thermal profile for a  $\dot{m} = 3 \times 10^4 \text{ g cm}^{-2} \text{ s}^{-1}$  ocean composed of  $^{16}\text{O}$ ,  $^{79}\text{Se}$  and with  $T = 2 \times 10^8 \text{ K}$  at  $\rho = 8 \times 10^5 \text{ g/cm}^3$ , both when the convective flux is included in the total heat flux  $F$  (solid line), and when it is ignored (i.e., the total heat flux is due only to the outward flux from the crust; dashed line).

Fig. 6 the thermal profile with and without the convective heating included, for an O-Se mixture with  $\dot{m}_4 = 3$  and  $T = 2 \times 10^8 \text{ K}$  at  $\rho = 8 \times 10^5 \text{ g/cm}^3$ .

## 5. DISCUSSION

We have explored the consequences of chemical separation in the ocean of accreting neutron stars. Given the rapid timescales for nucleation, growth, and sedimentation of solid particles, fluid elements that are lighter than their surrounding are continually being released at the base of the neutron star ocean. Using a mixing length model for convection, we modeled the resulting mixing zone. The conclusions are that the entire ocean is mixed, with a composition gradient  $\nabla_X \approx \chi T \nabla_{\text{ad}} / \chi_X \sim 100 k_B T / [\langle Z \rangle E_F]$  that is very shallow in the bulk of the ocean where the electrons are relativistically degenerate ( $E_F \gg k_B T$ ). The composition profile is therefore rather uniform and enhanced in light elements compared to the composition produced by nuclear burning of the accreted light elements at the top of the ocean. For example, for the largest charge ratio we considered, a mixture of O and Se, only 2% oxygen by mass was added to the ocean by nuclear burning, but the ocean itself is enriched in steady state to almost 40% by mass of oxygen (Fig. 2), set by the phase diagram for the O-Se mixture.

Accompanying the outwards transport of light elements is an inwards transport of heat. In §4, we argued that the ocean will evolve to a steady-state in which the convective heat flux is balanced by an outwards conductive flux. The effect of chemical separation is therefore to add a contribution to the outwards conductive heat flux in the ocean, steepening the temperature gradient. For the O-Se case, we find a heat flux of 0.2 MeV per nucleon at the base of the ocean, comparable to the flux expected from the crust. The heating is smaller for an Fe-Se ocean, which has a smaller contrast in composition between the two species. However, only a small amount of oxygen in the material entering the ocean is required to generate significant heating. In the O-Se case we considered, only 2% of the incoming mass is oxygen, compared to 40%

following enrichment. Therefore, in an ocean consisting of many species, even a small amount of light element entering the ocean could lead to significant heating through its enrichment. We are currently investigating the phase diagrams of multicomponent mixtures to assess the level of heating in that case.

An immediate application of our results is to superbursts. Following Horowitz et al. (2007) and Paper I, we chose oxygen as the light element for our example in this paper, but we have calculated models with carbon as the light element with similar results. Carbon enrichment through chemical separation at the base of the ocean, and subsequent upward mixing, could bring the carbon mass fraction  $X_C$  at the superburst ignition depth to within the required range  $X_C \approx 0.1$ – $0.2$  inferred from observations. Similarly, the heating associated with chemical separation will help to bring the temperature of the ocean up to the required ignition temperatures of  $5$ – $6 \times 10^8$  K. Questions still remain, however, such as whether this picture could match the observed recurrence times. The hotter ocean could also drive a heat flux into the outer crust, explaining the inverted temperature gradient found by Brown & Cumming (2009) in cooling transients. Time-dependent calculations of the evolution of the ocean are in progress to address these issues.

Compositionally-driven convection is important in cooling white dwarfs as well. The main difference between convection in the cores of cooling white dwarfs and in the oceans of accreting neutron stars is that in the white dwarf case a given mass element crosses the liquidus curve and crystallizes because the star cools, not because the element is pushed inwards. The similarities between these two systems are numerous. For example, the convectively stable composition gradient in the white dwarf interior is  $\nabla_{X,\text{WD}} \approx 0.03$ , nearly the same as the gradient in the neutron star ocean; the white dwarf crystallization rate,  $\dot{m}_{\text{WD}} \sim 0.1 \text{ g cm}^{-2} \text{ s}^{-1}$ , is also similar (Mochkovitch 1983). Therefore, we expect that much of our analysis and calculation from the present paper is applicable to the white dwarf case.

Another situation in which compositionally-driven convection is important is in the Earth’s core, in which chemical separation at the boundary between the liquid outer core and solid inner core drives convection in the outer core and provides an energy source for the Earth’s dynamo (Stevenson 1981). There are interesting differences between the Earth’s core and the neutron star ocean, however. First, the thermal gradient  $\nabla$  required to carry away the latent heat from the Earth’s inner-outer core boundary is significant, and exceeds  $\nabla_{\text{ad}}$ , so that the latent heat drives thermal convection. Second, in the Earth’s core  $\nabla_{\text{ad}} < \nabla_L$ , where  $\nabla_L$  is the liquidus temperature gradient (how the melting temperature varies with pressure). This allows the boundary between the inner and outer core to be at the melting temperature, but the outer core with an adiabatic profile remains above the melting temperature. Therefore a fluid thermally convecting outer core is possible (Loper & Roberts 1977; Stevenson 1980; the opposite was proposed by Higgins & Kennedy 1971 in what became known as the “core paradox”). In the neutron star ocean, however,  $\nabla_{\text{ad}} > \nabla_L$ : Equation (1) shows that for fixed  $\Gamma_i$ ,  $P \propto T^4$  so that  $\nabla_L = 0.25$ ; whereas using the results

of DeWitt & Slattery (2003) to calculate Coulomb corrections we find  $\nabla_{\text{ad}} \approx 0.36$  with a weak  $\Gamma_i$  dependence near the melting point. This means that the entire ocean could never be thermally convective and remain liquid.

The steady-state convective velocity is larger than the accretion velocity by a factor  $(X_b - X_0)/(X_b \nabla_X)$ , where  $X_b - X_0$  is the required change in composition across the ocean. Because the marginally-stable composition gradient in the ocean is very small, this factor is much greater than unity; in the deep ocean, this factor is of order 100. However, the corresponding velocity is still extremely slow such that additional processes that we have not considered here could change the picture we have put forward. For example, an extremely weak magnetic field (only about 100 G at the base of the ocean) would have an energy density comparable to the kinetic energy of the flow. The dipole magnetic fields of accreting neutron stars in low mass X-ray binaries are believed to be  $\sim 10^9$  G and stronger horizontal field components would not be surprising, e.g. due to screening currents (Cumming, Zweibel, & Bildsten 2001) or winding due to differential rotation and subsequent instabilities (Piro & Bildsten 2007). On a rotating star, Eddington-Sweet circulation in the ocean would have a timescale  $\sim t_{\text{therm}}(\Omega_B/\Omega)^2$  where  $\Omega_B$  is the break-up spin frequency. This timescale could be hundreds of days for a thermal time of days at the base of the ocean and  $\Omega/\Omega_B \approx 0.1$ , comparable to the convective turnover time. Further work is needed to investigate how rotational circulation or magnetic stresses would affect the models presented here.

The steady state we have been discussing is one in which the unstable composition gradient in the ocean is balanced by the stable temperature gradient, such that the ocean is only marginally unstable to convection. We find, however, that under certain conditions (e.g.,  $\dot{m} \geq \dot{m}_{\text{Edd}}$ ) the top of the ocean is thermally unstable to convection: the temperature gradient must satisfy  $\nabla > \nabla_{\text{ad}}$  in order to conduct away the large flux from the crust. In this case, either the convective velocity must be very large at the top of the ocean, or the unstable temperature gradient must be balanced by a *stable* composition gradient. The latter scenario is inconsistent with the two-component models of §3.1, where the fraction of the light element increases with depth; but could be consistent with the multicomponent models of §3.2 if the fraction of hydrogen-helium drops faster than oxygen or iron rises. We are currently studying the time-dependent case to understand what happens when  $\nabla > \nabla_{\text{ad}}$ .

In addition to oceans with thermally-driven convection, there are several other scenarios that are likely to lead to interesting time dependence of the mixing zone. For example, in transients in quiescence (see, e.g., Shternin et al. 2007; Brown & Cumming 2009) the mixing zone relaxes on a timescale comparable to the convective turnover time [Eq. (14)], about a month in the deep ocean. Mixing also occurs as the star cools after an accretion episode; the bulk of the ocean will solidify after a few days of cooling and will undergo chemical separation and further convection. Either of these effects could lead to late-time energy release, and provide a further observational test of the conditions in the ocean.

We thank Chuck Horowitz, Sanjay Reddy, and Chris Malone for useful discussions. We are grateful for support from NSERC and the Canadian Institute for Ad-

vanced Research (CIFAR). AC thanks the Kavli Institute for Astronomy and Astrophysics (KIAA) Beijing for hospitality during completion of this work.

#### REFERENCES

- Bildsten, L. & Cumming, A. 1998, *ApJ*, 506, 842  
 Bildsten, L. & Cutler, C. 1995, *ApJ*, 449, 800  
 Bildsten, L. & Hall, D. M. 2001, *ApJ*, 549, L219  
 Brown, E. F. 2000, *ApJ*, 531, 988  
 Brown, E. F. & Bildsten, L. 1998, *ApJ*, 496, 915  
 Brown, E. F., Bildsten, L., & Chang, P. 2002, *ApJ*, 574, 920  
 Brown, E. F. & Cumming, A. 2009, *ApJ*, 698, 1020  
 Cooper, R. L. & Bildsten, L. 2008, *Phys. Rev. E*, 77, 056405  
 Cox, J. P. 1980, *Theory of Stellar Pulsation* (Princeton: Princeton Univ. Press)  
 Cumming, A. & Bildsten, L. 2001, *ApJ*, 559, L127  
 Cumming, A., Macbeth, J., in 't Zand, J. J. M., & Page, D. 2006, *ApJ*, 646, 429  
 Cumming, A., Zweibel, E., & Bildsten, L. 2001, *ApJ*, 557, 958  
 Daligault, J. 2006a, *Phys. Rev. Lett.*, 96, 065003  
 Daligault, J. 2006b, *Phys. Rev. E*, 73, 056407  
 Daligault, J. & Murillo, M. S. 2005, *Phys. Rev. E*, 71, 036408  
 DeWitt, H. & Slattery, W. 2003, *Plasma Phys.*, 43, 279  
 Donkó, Z., & Nyíri, B. 2000, *Phys. Plasmas*, 7, 45  
 Gupta, S., Brown, E. F., Schatz, H., Möller, P., & Kratz, K.-L. 2007, *ApJ*, 662, 118  
 Hansen, C. J. & Kawaler, S. D. 1994, *Stellar Interiors: Physical Principles, Structure and Evolution* (New York: Springer Verlag)  
 Hansen, J.-P., McDonald, I. R., & Pollock, E. L. 1975, *Phys. Rev. A*, 11, 1025  
 Higgins, G. & Kennedy, G. C. 1971, *J. Geophys. Res.*, 76, 1870  
 Horowitz, C. J., Berry, D. K., & Brown, E. F. 2007, *Phys. Rev. E*, 75, 066101  
 Horowitz, C. J., Hughto, J., Schneider, A. S., & Berry, D. K. 2010, preprint (arXiv:1009.4248v1)  
 Ichimaru, S., Iyetomi, H., Mitake, S., & Itoh, N. 1983, *ApJ*, 265, L83  
 in 't Zand, J. J. M., Kuulkers, E., Verbunt, F., Heise, J., & Cornelisse, R. 2003, *A&A*, 411, L487  
 in 't Zand, J. J. M., Cumming, A., van der Sluys, M. V., Verbunt, F., & Pols, O. R. 2005, *A&A*, 441, 675  
 Keek, L., in 't Zand, J. J. M., Kuulkers, E., Cumming, A., Brown, E. F., & Suzuki, M. 2008, *A&A*, 479, 177  
 Kelton, K. F., Greer, A. L., & Thompson, C. V. 1983, *J. Chem. Phys.*, 79, 6261  
 Kippenhahn, R. & Weigert, A. 1994, *Stellar Structure and Evolution* (Springer-Verlag Berlin Heidelberg New York)  
 Kuulkers, E., in 't Zand, J. J. M., Homan, J., van Straaten, S., Altamirano, D., & van der Klis, M. 2004, in *AIP Conf. Proc.* 714, *X-Ray Timing 2003: Rossi and Beyond*, ed. P. Kaaret, F. K. Lamb, & J. H. Swank (Melville: AIP), 257  
 Loper, D. E. & Roberts, P. H. 1977, *Geophys. Astrophys. Fluid Dynamics*, 9, 289  
 Medin, Z. & Cumming, A. 2010, *Phys. Rev. E*, 81, 036107  
 Mochkovitch, R. 1983, *A&A*, 122, 212  
 Montgomery, M. H., Klumpe, E. W., Winget, D. E., & Wood, M. A. 1999, *ApJ*, 525, 482  
 Paczyński, B. 1983, *ApJ*, 267, 31  
 Peng, F., Brown, E. F., & Truran, J. W. 2007, *ApJ*, 654, 1022  
 Piro, A. L., & Bildsten, L. 2005, *ApJ*, 619, 1054  
 Piro, A. L. & Bildsten, L. 2007, *ApJ*, 663, 1252  
 Potekhin, A. Y. & Chabrier, G. 2000, *Phys. Rev. E*, 62, 8554  
 Schatz, H., Aprahamian, A., Barnard, V., Bildsten, L., Cumming, A., Ouellette, M., Rauscher, T., Thielemann, F.-K., & Wiescher, M. 2001, *Phys. Rev. Lett.*, 86, 3471  
 Schatz, H., Bildsten, L., Cumming, A., & Ouellette, M. 2003, *Nucl. Phys. A*, 718, 247  
 Shternin, P. S., Yakovlev, D. G., Haensel, P., & Potekhin, A. Y. 2007, *MNRAS*, 382, 43  
 Stevenson, D. J. 1980, *Physics of the Earth and Planetary Interiors*, 22, 42  
 Stevenson, D. J. 1981, *Science*, 214, 611  
 Strohmayer, T. E., & Brown, E. F. 2002, *ApJ*, 566, 1045  
 Vehkamäki, H. 2006, *Classical nucleation theory in multicomponent systems* (Springer-Verlag: Berlin Heidelberg)  
 Woosley, S. E., Heger, A., Cumming, A., Hoffman, R. D., Pruet, J., Rauscher, T., Fisker, J. L., Schatz, H., Brown, B. A., & Wiescher, M. 2004, *ApJS*, 151, 75  
 Yakovlev, D. G. & Urpin, V. A. 1980, *Soviet Ast.*, 24, 303